

Supporting Information

Reference 28

Frisch, M. J.; Trucks, G. W.; Schlegel, H. B.; Scuseria, G. E.; Robb, M. A.; Cheeseman, J. R.; J. A. Montgomery, J.; Vreven, T.; Kudin, K. N.; Burant, J. C.; Millam, J. M.; Iyengar, S. S.; Tomasi, J.; Barone, V.; Mennucci, B.; Cossi, M.; Scalmani, G.; Rega, N.; Petersson, G. A.; Nakatsuji, H.; Hada, M.; Ehara, M.; Toyota, K.; Fukuda, R.; Hasegawa, J.; Ishida, M.; Nakajima, T.; Honda, Y.; Kitao, O.; Nakai, H.; Klene, M.; Li, X.; Knox, J. E.; Hratchian, H. P.; Cross, J. B.; Adamo, C.; Jaramillo, J.; Gomperts, R.; Stratmann, R. E.; Yazyev, O.; Austin, A. J.; Cammi, R.; Pomelli, C.; Ochterski, J. W.; Ayala, P. Y.; Morokuma, K.; Voth, G. A.; Salvador, P.; Dannenberg, J. J.; Zakrzewski, V. G.; Dapprich, S.; Daniels, A. D.; Strain, M. C.; Farkas, O.; Malick, D. K.; Rabuck, A. D.; Raghavachari, K.; Foresman, J. B.; Ortiz, J. V.; Cui, Q.; Baboul, A. G.; Clifford, S.; Cioslowski, J.; Stefanov, B. B.; Liu, G.; Liashenko, A.; Piskorz, P.; Komaromi, I.; Martin, R. L.; Fox, D. J.; Keith, T.; Al-Laham, M. A.; Peng, C. Y.; Naayakkara, A.; Challacombe, M.; Gill, P. M. W.; Johnson, B.; Chen, W.; Wong, M. W.; Gonzalez, C.; Pople, J. A., *Gaussian 03, Revisions C.01 and E.01*, Wallingford, CT, 2004.

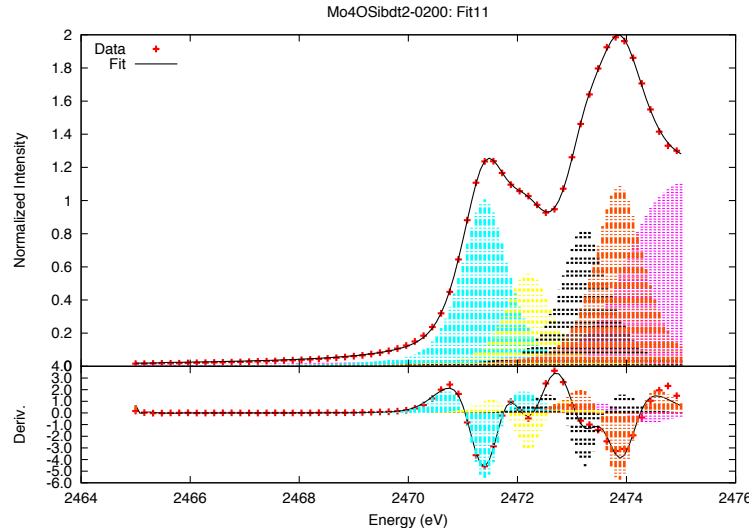


Figure S1: Fit to normalized data and second derivative of $[\text{Mo}(\text{OSi})(\text{bdt})_2]^{1-}$.

Table S1: Parameters for fit of $[\text{Mo}(\text{OSi})(\text{bdt})_2]^{1-}$. The first four rows correspond to peaks while the last row corresponds to the rising edge.

Energy (eV)	Amplitude	Width	Area
2471.40	1.008	0.504	1.017
2472.16	0.567	0.504	0.572
2473.24	0.841	0.514	0.866
2473.86	1.094	0.528	1.155
2473.94	1.104	0.594	—

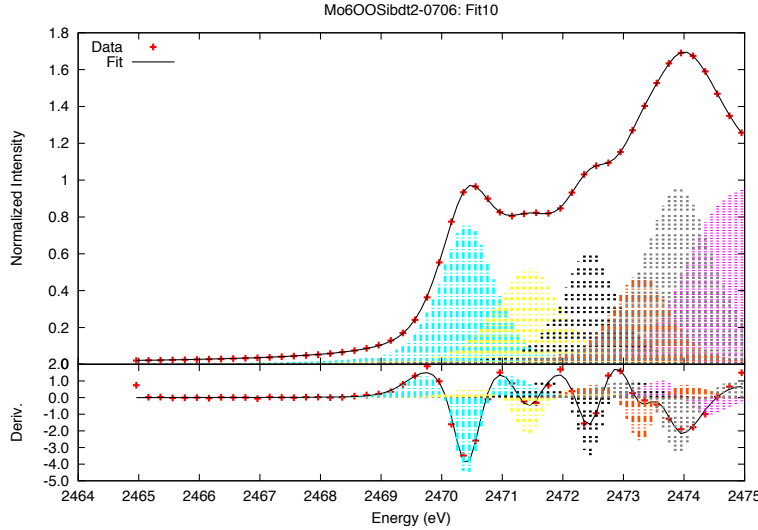


Figure S2: Fit to normalized data and second derivative of $[\text{MoO}(\text{OSi})(\text{bdt})_2]^{1-}$.

Table S2: Parameters for fit of $[\text{MoO}(\text{OSi})(\text{bdt})_2]^{1-}$. The first five rows correspond to peaks while the last row corresponds to the rising edge.

Energy (eV)	Amplitude	Width	Area
2470.41	0.768	0.528	0.811
2471.43	0.524	0.642	0.673
2472.44	0.618	0.544	0.672
2473.28	0.493	0.562	0.554
2473.91	0.960	0.698	1.339
2474.00	1.022	0.525	—

Table S3: Comparison of structural parameters of the geometry optimized (DFT) and crystallographic structures.

	$[\text{Mo}(\text{OSi})(\text{bdt})_2]^{1-}$		$[\text{MoO}(\text{OSi})(\text{bdt})_2]^{1-}$	
	Crystal	DFT	Crystal	DFT
Mo-S1 (\AA)	2.34	2.37	2.43	2.47
Mo-S2 (\AA)	2.34	2.37	2.41	2.44
Mo-S3 (\AA)	2.34	2.37	2.44	2.46
Mo-S4 (\AA)	2.34	2.37	2.49	2.57
Mo-O (\AA)	1.84	1.86	1.93	1.94
Mo=O (\AA)	-	-	1.71	1.70
θ ($^\circ$)	143.4	143.4	152.8	157.5
ϕ ($^\circ$)	178.8	179.8	109.2	106.6

Table S4: Molecular Orbital Composition (%) Near the HOMO-LUMO Gap^a

		Mo d	Mo s	Mo p	S p	O(Si)	O	C/H
$[\text{Mo}(\text{mdt})_3]^{2-}$	Mo d_{xz}/d_{yz}	52	0	0	41	-	-	7
	Mo $d_{x^2-y^2}/d_{xy}$	52	0	0	38	-	-	8
	L π_{AB}^+	0	0	0	70	-	-	30
	Mo d_{z^2}	71	1	0	10	-	-	13
$[\text{Mo}(\text{mdt})_3]$	Mo d_{xz}/d_{yz}	53	0	0	40	-	-	6
	Mo $d_{x^2-y^2}/d_{xy}$	49	0	1	42	-	-	6
	L π_{AB}^+	15	0	0	54	-	-	30
	Mo d_{z^2}	63	1	0	11	-	-	18
$[\text{Mo}(\text{OSi})(\text{bdt})_2]^{1-}$	Mo d_{xy}	52	0	0	45	0	-	2
	Mo d_{z^2}	55	0	8	18	6	-	11
	Mo d_{xz}	62	0	0	26	6	-	6
	Mo d_{yz}	62	0	0	19	7	-	11
	Mo $d_{x^2-y^2}$	78	0	0	6	0	-	11
	L π_{AB}^+	3	0	0	51	2	-	44
$[\text{MoO}(\text{OSi})(\text{bdt})_2]^{1-}$	Mo d_{z^2}	44	6	4	23	4	13	3
	Mo d_{xy}	47	0	0	35	2	1	11
	Mo d_{xz}	58	0	1	17	1	18	4
	Mo d_{yz}	60	0	1	8	3	20	6
	Mo $d_{x^2-y^2}$	49	0	0	32	7	1	10
	L π_{AB}^+	2	0	0	54	2	2	39

^aUnoccupied orbitals are shown in bold

Table S5: Comparison of structural parameters of the geometry optimized (DFT) structures between Mo(IV) and Mo(VI)=O complexes with truncated axial and dithiolene ligands.

	[Mo(OSi)(bdt) ₂] ¹⁻	[Mo(OMe)(mdt) ₂] ¹⁻	[MoO(OSi)(bdt) ₂] ¹⁻	MoO(OMe)(mdt) ₂] ¹⁻
Mo-S1 (Å)	2.37	2.36	2.47	2.48
Mo-S2 (Å)	2.37	2.36	2.44	2.44
Mo-S3 (Å)	2.37	2.37	2.46	2.44
Mo-S4 (Å)	2.37	2.37	2.57	2.57
Mo-O (Å)	1.86	1.87	1.94	1.96
Mo=O (Å)	—	—	1.70	1.71
θ (°)	143.4	144.8	157.5	158.8
ϕ (°)	179.8	180.0	106.6	109.3

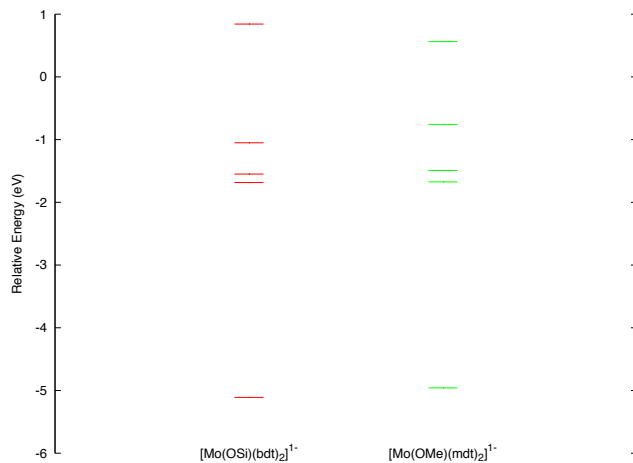


Figure S3: Molecular orbital diagram for $[\text{Mo}(\text{OSi})(\text{bdt})_2]^{1-}$ (left) and $[\text{Mo}(\text{OMe})(\text{mdt})_2]^{1-}$ (right).

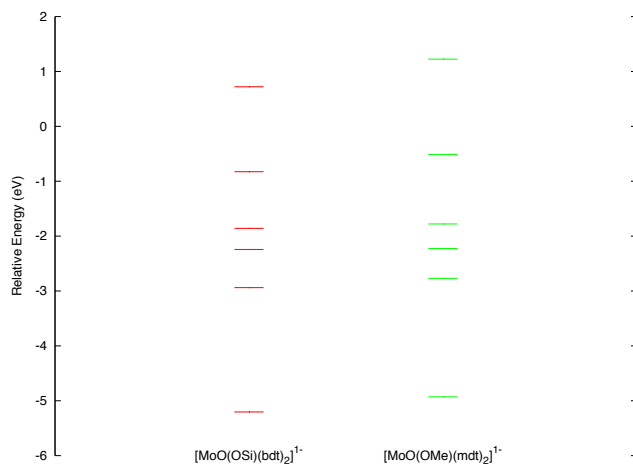


Figure S4: Molecular orbital diagram for $[\text{MoO}(\text{OSi})(\text{bdt})_2]^{1-}$ (left) and $[\text{MoO}(\text{OMe})(\text{mdt})_2]^{1-}$ (right).

Table S6: Molecular Orbital Composition (%) Near the HOMO-LUMO Gap^a

		Mo d	Mo s	Mo p	S p	O(Si)	O	C/H
[Mo(OMe)(mdt) ₂] ¹⁻	Mo d_{xy}	52	0	0	47	0	-	2
	Mo d_{z²}	55	3	8	19	8	-	5
	Mo d_{yz}	63	0	0	17	9	-	9
	Mo d_{xz}	59	0	1	29	3	-	6
	Mo d _{x²-y²}	76	0	0	7	0	-	12
	L π _{AB} ⁺	7	0	0	46	2	-	44
[MoO(OMe)(mdt) ₂] ¹⁻	Mo d_{z²}	46	6	3	20	7	15	3
	Mo d_{xy}	49	0	0	38	3	1	8
	Mo d_{xz}	58	0	1	18	1	17	4
	Mo d_{yz}	62	0	1	8	3	21	5
	Mo d _{x²-y²}	47	0	0	34	8	1	9
	L π _{AB} ⁺	3	0	0	52	2	3	40

^aUnoccupied orbitals are shown in bold